Computational Mechanics
https://doi.org/10.1007/s00466-024-02467-3

ORIGINAL PAPER

A machine-learning enabled digital-twin framework for the rapid design of satellite constellations for "Planet-X"

T. I. Zohdi[1]

Received: 12 January 2024 / Accepted: 21 February 2024

Abstract
Worldwide communication bandwidth growth has largely been driven by (1) multimedia demands, (2) multicommunication-point demands and (3) multicommunication-rate demands, and has increased dramatically over the last two decades due to e-commerce, internet communication and the explosion of cell-phone use, in particular for in-flight services, all of which necessitate broadband use and low latency. In order to accommodate this huge surge in demand, next generation "mega-constellations" of satellites are being proposed combining a mix of heterogeneous unit types in LEO, MEO and GEO orbital shells, in order to provide continuous lower-latency and high-bandwidth service which exploits a wide-range of frequencies for fast internet connections (broadband, which is not possible with single satellite-type orbital shell systems). Accordingly, in this work, we develop a computationally-efficient digital-twin framework for a constellation of satellites around an arbitrary planet ("Planet-X"). The rapid speed of these simulations enables the ability to explore satellite infrastructure parameter combinations, represented by a multicomponent satellite constellation design vector $\boldsymbol{\Lambda} \stackrel{\text{def}}{=}$ (number of satellites, satellite orbital radii, satellite orbital speeds, satellite types), that can deliver desired communication signal or camera coverage on "Planet-X", while simultaneously incorporating satellite infrastructural resource constraints. In order to cast the objective mathematically, we set up the system design as an inverse problem to minimize a cost function via a Genetic Machine Learning Algorithm (G-MLA), which is well-suited for nonconvex optimization. Numerical examples are provided to illustrate the framework.

Keywords Constellations · Satellites · Machine-learning

1 Constellations of satellites

A satellite constellation is defined as a system of artificial satellites which provides continuous global coverage over a planet. This eliminates two key problems encountered with single satellite systems, namely intermittent coverage and the lack of backup redundancy. The key components of a satellite constellation infrastructure are:

- Number of satellites,
- Satellite orbital shells,
- Satellite orbital speeds and
- Satellite types.

Satellite constellations are fundamentally different to satellite clusters, which orbit as a group in a fixed formation, and to satellite fleets, where each satellite operates individually. Most satellites perform missions that fall into one of three categories: planet observation, navigation, or communications. There are almost 10,000 active satellites in Earth's orbit as of the end of 2023 and it is estimated that 60,000 will be in operation by 2030. The majority of satellites operate in a circular orbit, in three main classes (Figs. 1, 2 and 3):

- Low Earth Orbit (LEO): 300–2000 km in altitude, which are usually less expensive and have shorter useful operational lifetimes, relative to higher-altitude satellites. Since they travel at much higher speeds, and at lower-altitudes, their coverage is shorter and more limited than higher-altitude satellites, illustrated by summing the centripetal and gravitational forces in the radial direction for a stable circular orbit for jth satellite

✉ T. I. Zohdi
zohdi@berkeley.edu

[1] Department of Mechanical Engineering, University of California, 6117 Etcheverry Hall, Berkeley, CA 94720-1740, USA

Published online: 12 April 2024

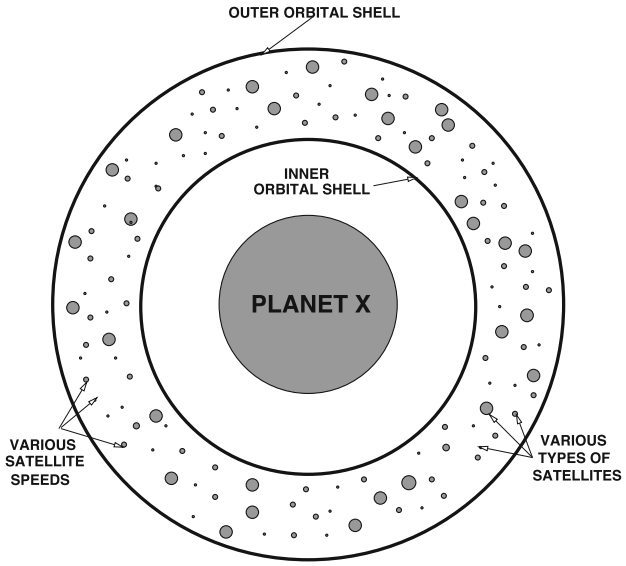

Fig. 1 Parameters in a satellite constellation comprised of a variety of heterogeneous satellites in varying orbital shells with varying rotational velocities

$$m_j \frac{d^2 r_j}{dt^2} = -m_j \frac{v_j^2}{r_j} = -\frac{G M_e m_j}{r_j^2} = 0 \Rightarrow v_j = \sqrt{\frac{G M_e}{r_j}}, \tag{1.1}$$

where m_j is the mass of the satellite, r_j is the radius of the satellite orbit, M_e is the mass of Earth and G is the universal gravitational constant. To illustrate the dimensionality of such systems, the International Space Station orbits at about 400 km and Iridium, a satellite phone provider, orbits its satellites at about 780 km, while a commercial passenger aircraft flies at an altitude of about 10 km. The International Space Station travels at about 7.7 km per second.

- Medium Earth Orbit (MEO): 2000–35,000 km in altitude and is more expensive to launch and maintain, but still requires constellations for complete coverage, despite having longer and larger coverage than individual LEO satellites. Most MEO satellites, however, orbit at an altitude of between 18,000–24,000 km, for example the GPS constellation orbits at 20,200 km.
- Geosynchronous Earth Orbit (GEO): 35,786 km in altitude, chosen so that the satellite moves at the same angular velocity as Earth's rotation ($\omega_j = \omega_e$), so it appears still (with period of one sidereal day), achieved by setting the velocity of a satellite to be $v = r_j \omega_e$ in Eq. (1.1):

$$v_j = r_j \omega_e = \sqrt{\frac{G M_e}{r_j}} \Rightarrow r_j = \left(\frac{G M_e}{\omega_e^2} \right)^{1/3}, \tag{1.2}$$

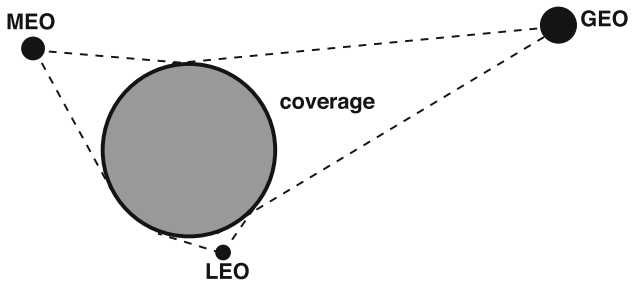

Fig. 2 Coverage by LEO, MEO and GEO systems (not drawn to scale)

where ω_e is the angular velocity of Earth's rotation. A satellite orbiting directly over the equator will remain above the same ground location throughout its orbit, which is referred to as a Geostationary orbit, while a Geosynchronous orbit wanders slightly, but returns to the same location at the same time each day, with an orbital period of 23 h, 56 min and 4 s. Satellites in GEO travel at about 3.1 km per second. To attain geosynchronous Earth orbit (a) a spacecraft is first launched into an elliptical orbit with apoapsis altitude of approximately 35,786 km (this is the geosynchronous transfer orbit) and (b) the rocket then circularizes the orbit by turning parallel to the equator and firing its rocket engines (apogee motor). We note that a Graveyard orbit is achieved when a satellite is to be decommissioned-*it is pushed to geosynchronous orbit plus 300 km.*

Low Earth Orbit (LEO) constellations have thus far been the most common, with the driving factors being that

- They are the least expensive to maintain and launch,
- They have lower communication latency than larger orbits, such as MEO or GEO,
- They have lower power requirements and
- They are necessary because of the limitation of smaller coverage of a single LEO satellite (Figs. 2 and 3).

Prominent examples of satellite constellations include Starlink, Iridium, Globalstar, Orbcomm communications in LEO and Global Positioning System (GPS), Galileo and GLONASS for navigation in MEO. There are a variety of classical constellation patterns [such as the Walker Delta and Star Patterns (Walker [1, 2])] that are used for such systems, however, they make assumptions about regular patterns, similar orbital shells, etc. In general, the farther a satellite is from the Earth's surface, the more sophisticated the satellite equipment needs to be to perform its mission, thus, LEO satellites generally cost less than those in larger orbits and have simpler and less power-intensive payloads. Generally, satellites with smaller payloads have correspondingly lower mass and cost

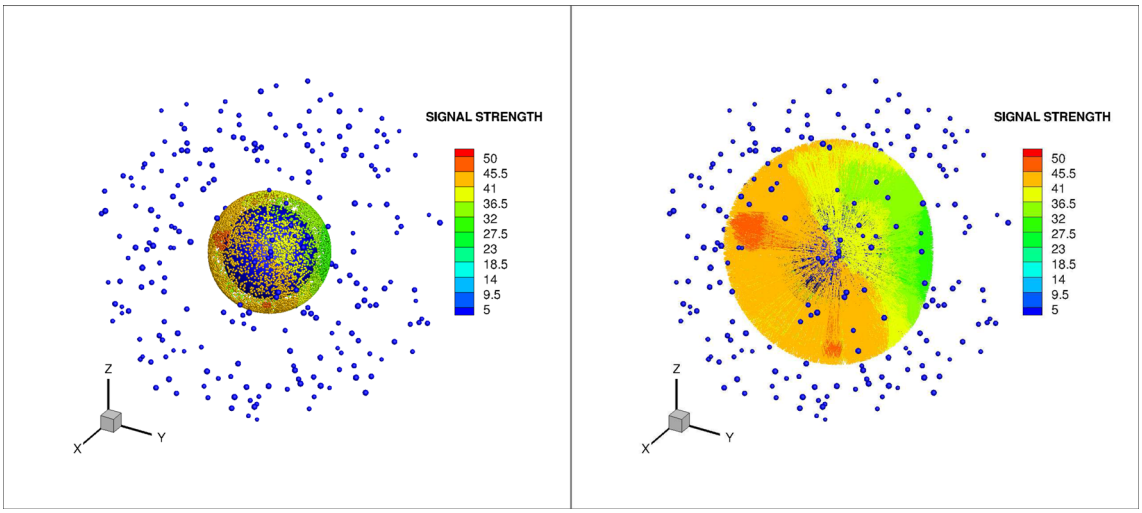

Fig. 3 Left: ground stations and distribution of different sized satellites, each with different orbits (all circular in this case) and varying speeds (from upcoming simulations described later). Right: signal strengths (nondimensional)shown on the surface of Planet-X are the signal strengths received from all of the satellites

less than those with higher mass. Additionally, LEO launch costs are lower because less energy is required to lift satellites to lower altitudes. Thus, in summary, LEO satellites are less expensive than larger MEO and GEO satellites, but are less capable.

1.1 Objectives

Worldwide communication bandwidth growth has largely been driven by (1) multimedia demands, (2) multicommunication-point demands and (3) multicommunication-rate demands, which has increased dramatically over the last two decades due to e-commerce, internet communication and the explosion of cell-phone use, in particular for in-flight services, all of which necessitate broadband use and low latency. The term "broadband" is synonymous with high-speed internet, as currently defined by the US Federal Communications Commission (FCC) as a minimum of 25 Megabits per second (Mbps) download and 3 Mbps upload. Broadband is a high-capacity transmission technique using a wide range of frequencies, which enables a large number of messages to be communicated simultaneously. In order to accommodate this huge surge in demand, next generation satellite "megaconstellations" are being proposed combining a mix of different satellite types in LEO, MEO and GEO orbital shells, in order to provide continuous low-latency and high-bandwidth service which exploits a wide-range of frequencies for fast internet connections (broadband is difficult with single satellite-type orbital shell systems). This motivates multiple orbital shells and a variety of satellite types, etc. Most notably, Starlink plans to have 12,000 satellites by 2026 in multiple orbital shells. For a wide survey and cross-section of the literature on satellite constellations, see Curzi et al. through Polishuk et al. [3–56]. Accordingly, in this work, we develop a computationally-efficient digital-twin framework for a constellation of satellites around an arbitrary planet ("Planet-X", Fig. 1). The high speed of such simulations enables the ability to explore which satellite infrastructure parameter combinations, represented by a multicomponent satellite constellation design vector $\mathbf{\Lambda} \stackrel{\text{def}}{=}$ (number of satellites, satellite orbital radii, satellite orbital speeds, satellite types), can deliver desired communication signal or camera coverage on "Planet-X", while simultaneously incorporating satellite infrastructural resource constraints. In order to cast the objective mathematically, we set up the system design as an inverse problem to minimize a cost function via a Genetic Machine Learning Algorithm (G-MLA), which is well-suited for nonconvex optimization. Numerical examples are provided to illustrate the framework.

2 Fundamentals of satellite dynamics

2.1 Newton's law of gravitation for multiple bodies

The fundamental equation for gravitational interaction between bodies is given by (Fig. 4, ignoring relativistic effects)

$$\boldsymbol{F}_i^{grav} = -\boldsymbol{F}_j^{grav} = -\frac{Gm_i m_j}{||\boldsymbol{r}_{j\to i}||^2}\underbrace{\frac{\boldsymbol{r}_{j\to i}}{||\boldsymbol{r}_{j\to i}||}}_{\boldsymbol{n}_{j\to i}} = -\frac{Gm_i m_j}{||\boldsymbol{r}_{j\to i}||^3}\boldsymbol{r}_{j\to i}. \tag{2.1}$$

For multiple bodies, $j = 1, 2, \ldots, N^s$, the force on i is

$$\boldsymbol{F}_i^{grav,tot} = -\sum_{j=1, j\neq i}^{N} \frac{Gm_i m_j}{||\boldsymbol{r}_{j\to i}||^2} \underbrace{\frac{\boldsymbol{r}_{j\to i}}{||\boldsymbol{r}_{j\to i}||}}_{\boldsymbol{n}_{j\to i}} = -\sum_{j=1, j\neq i}^{N} \frac{Gm_i m_j}{||\boldsymbol{r}_{j\to i}||^3} \boldsymbol{r}_{j\to i} = -\boldsymbol{F}_j^{grav,tot}. \quad (2.2)$$

The governing equation for motion becomes

$$\frac{d(m_j \boldsymbol{v}_j)}{dt} = \boldsymbol{F}_j^{grav,tot} + \boldsymbol{F}_j^{other} \stackrel{\text{def}}{=} \boldsymbol{F}_j^{ext} \quad (2.3)$$

where $\boldsymbol{F}_j^{other}$ accounts for thrust, drag, etc. and $\boldsymbol{F}_j^{ext}$ is the total of the external forces.

2.2 Simplifying assumptions for the unilateral 2-body problem

We make a number of simplifying assumptions (Fig. 4)

- The losses in mass are negligible: $\frac{dm_j}{dt} \approx 0$,
- There is one dominant gravitational source: Planet-X,
- The coordinate system is centered at Planet-X's center; assumed stationary.

These assumptions lead to ($||\boldsymbol{r}_j|| = r_j$)

$$m_j \dot{\boldsymbol{v}}_j = \boldsymbol{F}_j^{other} - \frac{GM_{px}m_j}{r_j^3}\boldsymbol{r}_j \stackrel{\text{def}}{=} \boldsymbol{F}_j^{ext}. \quad (2.4)$$

Later in the work, we will discuss other key aspects of classical orbital mechanics of satellites.

2.3 Governing equations for satellite dynamics in two dimensions

Referring to Fig. 5, for an object with position vector $\boldsymbol{r}_j$, general 2D (orbital plane) motion is given by

$$\boldsymbol{r}_j = r_j \boldsymbol{e}_r, \quad (2.5)$$

where r_j is the magnitude of $\boldsymbol{r}_j$ and $\boldsymbol{e}_r$ is the radial unit vector, which leads to

$$\boldsymbol{v}_j = \dot{\boldsymbol{r}}_j = \dot{r}_j \boldsymbol{e}_r + r_j \dot{\boldsymbol{e}}_r = \dot{r}_j \boldsymbol{e}_r + r_j \dot{\theta}_j \boldsymbol{e}_\theta, \quad (2.6)$$

where $\boldsymbol{v}_j$ is the velocity and θ_j is the angular coordinate and e_θ is the angular unit vector, which yields the acceleration ($\boldsymbol{a}_j$)

$$\boldsymbol{a}_j = \dot{\boldsymbol{v}}_j = \ddot{\boldsymbol{r}}_j = \ddot{r}_j \boldsymbol{e}_r + r_j \boldsymbol{e}_r + \dot{r}_j \dot{\theta}_j \boldsymbol{e}_\theta + r_j \ddot{\theta}_j \boldsymbol{e}_\theta + r_j \dot{\theta}_j \boldsymbol{e}_\theta = (\ddot{r}_j - r_j \dot{\theta}_j^2)\boldsymbol{e}_r + (r_j \ddot{\theta}_j + 2\dot{r}_j \dot{\theta}_j)\boldsymbol{e}_\theta. \quad (2.7)$$

This leads to the following governing equations

$$m_j(\ddot{r}_j - r\dot{\theta}_j^2) = F_{jr}^{other} - \frac{GM_{px}m_j}{r_j^2} \quad (2.8)$$

and

$$m_j(r_j \ddot{\theta}_j + 2\dot{r}_j \dot{\theta}_j) = F_{j\theta}^{other}. \quad (2.9)$$

2.4 Governing equations for satellite dynamics in three dimensions

The extension to 3D, starts similarly with (Fig. 5)

$$\boldsymbol{r}_j = r_j \boldsymbol{e}_r, \quad (2.10)$$

which yields

$$\boldsymbol{v}_j = \dot{r}_j \boldsymbol{e}_r + r_j \dot{\theta}_j \sin\phi_j \boldsymbol{e}_\theta + r_j \dot{\phi}_j \boldsymbol{e}_\phi, \quad (2.11)$$

which leads to

$$\begin{aligned}\boldsymbol{a}_j = \dot{\boldsymbol{v}}_j = \ddot{\boldsymbol{r}}_j = {} & (\ddot{r}_j - r_j\dot{\theta}_j^2 \sin^2\phi_j - r_j\dot{\phi}_j^2)\boldsymbol{e}_r \\ & + (r_j\ddot{\theta}_j \sin\phi_j + 2\dot{r}_j\dot{\theta}_j \sin\phi_j \\ & + 2r_j\dot{\theta}_j \cos\phi_j)\boldsymbol{e}_\theta + (r_j\ddot{\phi}_j + 2\dot{r}_j\dot{\phi}_j \\ & - r_j\dot{\theta}_j^2 \sin\phi_j \cos\phi_j)\boldsymbol{e}_\phi. \end{aligned} \quad (2.12)$$

This provides the following governing equations

$$m_j(\ddot{r}_j - r_j\dot{\theta}_j^2 \sin^2\phi_j - r_j\dot{\phi}_j^2) = F_{jr}^{other} - \frac{GM_{px}m_j}{r_j^2} \quad (2.13)$$

and

$$m_j(r_j\ddot{\theta}_j \sin\phi_j + 2\dot{r}_j\dot{\theta}_j \sin\phi_j + 2r_j\dot{\theta}_j \cos\phi_j) = F_{j\theta}^{other} \quad (2.14)$$

and

$$m_j(r_j\ddot{\phi}_j + 2\dot{r}_j\dot{\phi}_j - r_j\dot{\theta}_j^2 \sin\phi_j \cos\phi_j) = F_{j\phi}^{other}. \quad (2.15)$$

2.5 Numerical methods (for any coordinate system)

Generally, when numerical methods are employed, Cartesian formulations are preferred. For example, consider

$$m_j \dot{\boldsymbol{v}}_j = \boldsymbol{F}_j^{ext}, \quad (2.16)$$

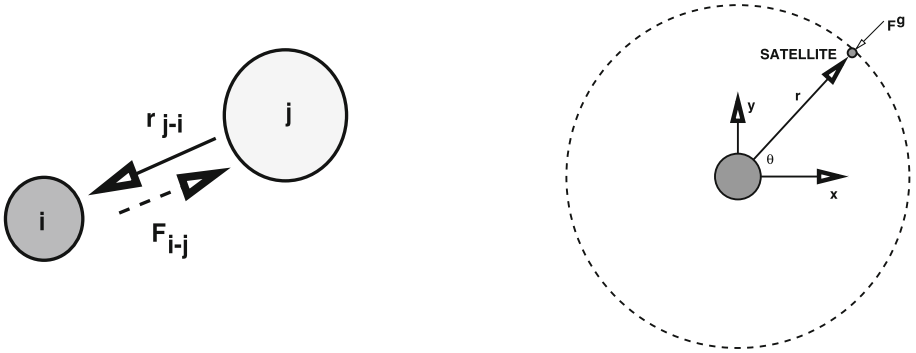

Fig. 4 The basis of gravitational interaction and the Planet-X-satellite system

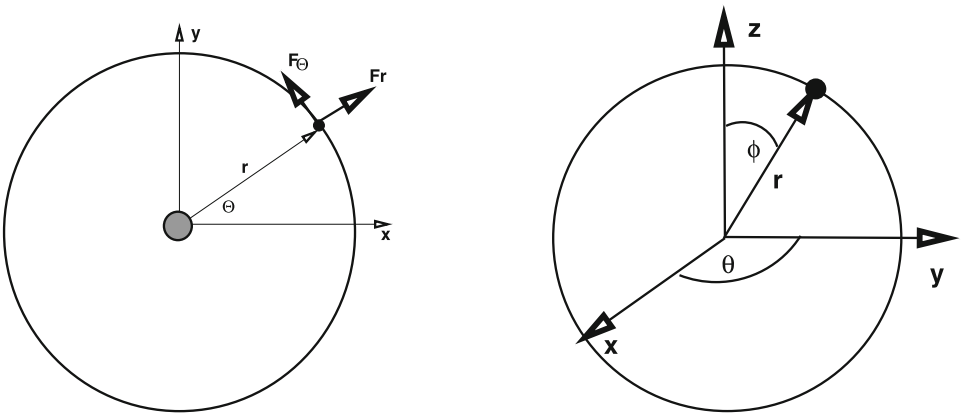

Fig. 5 Nomenclature for equations of motion and spherical coordinates for 3D orbits

where $\boldsymbol{F}_j^{ext}$ is a general force vector comprising gravity, thrust adjustment forces, etc., yielding, with explicit time stepping

$$\frac{\boldsymbol{v}_j(t+\Delta t)-\boldsymbol{v}_j(t)}{\Delta t} \approx \frac{1}{m_j}\boldsymbol{F}_j^{ext}(t) \Rightarrow \boldsymbol{v}_j(t+\Delta t) = \boldsymbol{v}_j(t) + \frac{\Delta t}{m_j}\boldsymbol{F}_j^{ext}(t). \tag{2.17}$$

By the same approach, for the position vector

$$\frac{\boldsymbol{r}_j(t+\Delta t)-\boldsymbol{r}_j(t)}{\Delta t} \approx \boldsymbol{v}_j(t) \Rightarrow \boldsymbol{r}_j(t+\Delta t) = \boldsymbol{r}_j(t) + \Delta t\boldsymbol{v}_j(t). \tag{2.18}$$

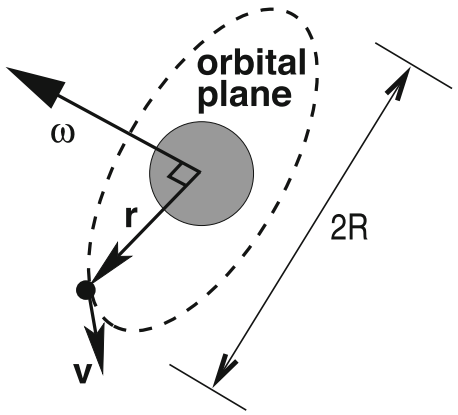

Fig. 6 Generation of an orbital plane

2.6 Steady-state circular orbits

In the case of a steady-state planar circular orbit, simplified dynamics follow (the coordinate system is centered at Planet-X's center, also assumed stationary):

- One generates an orbital plane at a prescribed angle (Fig. 6),
- Place the angular velocity vector at the center of "Planet-X",
- Compute the instantaneous orbital velocity vector, $\boldsymbol{v}_j(t) = \boldsymbol{\omega}_j \times \boldsymbol{r}_j(t)$,
- Increment the predicted position, $\hat{\boldsymbol{r}}_j(t+\Delta t) = \boldsymbol{r}_j(t) + \Delta t\boldsymbol{v}_j(t)$,
- Compute the altitude correction (radial return), $\boldsymbol{r}_j(t+\Delta t) = r_j\left(\frac{\hat{\boldsymbol{r}}_j(t+\Delta t)}{||\hat{\boldsymbol{r}}_j(t+\Delta t)||}\right)$, where r_j is the orbital radius.

The direct altitude correction to attain a perfectly circular orbit replaces the need for the force-based formulation (Eq. 2.17), where the forces would counteract losses due to

gravitational pull and drag. This is more direct, simpler and exact, due to the assumption of a circular orbit. Later in the work, we consider power to maintain circular orbits at prescribed speeds as well as general (noncircular) orbits.

3 Objectives and model problem

3.1 Overview

We now construct a cost function which represents (1) the coverage of the planet by the constellation and (2) the expense of deploying and maintaining the constellation. The coverage of the planet is relatively straightforward, since it is essentially geometric (Fig. 3), although the coverage quality will decay with distance, which we embed into the performance metrics via an exponential decay of coverage strength. The costs associated with the expense of deploying and maintaining the constellation will be simplified, using the following general trends:

- More satellites makes the system more expensive to manufacture and to manage in orbit,
- Larger orbits provide better coverage, but are more expensive, due to launch power needed for larger orbits,
- Faster traveling satellites are more expensive, due to the power needed to maintain faster orbital speeds and
- Larger satellites provide better coverage, but are more expensive, due to launch power needed and more power needed to operate and maintain orbit.

These are generalized simplifications, since there is potentially significant coupling between these trends. Furthermore, there is an expense in maintaining a circular orbit at a certain speed (see Eq. 1.1), balanced by possible solar recharging features. A more detailed framework would need to focus on the specific type of satellites deployed, which is outside the scope of the current work, but will be discussed further in the summary. In order to cast the objective mathematically, we set up an inverse problem as a Machine Learning Algorithm (MLA); specifically a Genetic MLA (G-MLA) variant, which is well-suited for nonconvex optimization.

3.2 Overall algorithm

The algorithm is as follows for as population of N_i^g ground sites to be covered ($i = 1, 2, \ldots N^g$) on the surface of Planet-X.

- **STEP 1**: For the constellation Infrastructure (Fig. 7), there are 4 key parameters, the number of satellites, the satellite orbits, the satellite orbital angular velocities and the satellite sizes ($0 \leq RAND \leq 1$):
  - Satellite number: $N_o^s \leq N_j^s \leq N^{s,max}$, where $N_j^s = N_o^s + (N^{s,max} - N_o^s) \times RAND_j$,
  - Satellite orbital radii: $r_o^s \leq r_j^s \leq r_o^s \times (1 + (\Delta r^s - 1) \times RAND_j)$, where $1 \leq \Delta r^s \leq \Delta r^{s,max}$,
  - Satellite orbital speeds: $\omega_o^s \leq \omega_j^s \leq \omega_o^s \times (1 + (\Delta \omega^s - 1) \times RAND_j)$, where $1 \leq \Delta \omega^s \leq \Delta \omega^{s,max}$ and
  - Satellite sizes: $L_o^s \leq L_j^s \leq L_o^s \times (1 + (\Delta L^s - 1) \times RAND_j)$, where $1 \leq \Delta L^s \leq \Delta L^{s,max}$.
- **STEP 2**: Using the methods described in the previous section (for circular orbits), compute the dynamics of the bodies $j = 1, 2, \ldots, N^s$, for the time period selected $\boldsymbol{r}_j(t), \boldsymbol{r}_j(t + \Delta t), \boldsymbol{r}_j(t + 2\Delta t), \ldots, \boldsymbol{r}_j(T)$ (Fig. 7).
- **STEP 3**: Extract the following orbital quantities:
- The received ground signal strength for ground site i, scaled by the smallest satellite size m_o, with exponential distance decay (Fig. 7):

$$S_{i/j}^g = \underbrace{S_o}_{\text{nominal signal strength}} \times \underbrace{\frac{m_j}{m_o}}_{\text{satellite size scaling}} \times \underbrace{\frac{I_{i/j}}{||\boldsymbol{r}_j^s - \boldsymbol{r}_i^g||}}_{\text{overhead scaling}} \times \underbrace{e^{-d||\boldsymbol{r}_j^s - \boldsymbol{r}_i^g||}}_{\text{distance decay}}, \tag{3.1}$$

where S_o is the signal strength, which is unit less for the purposes of this model problem, but could represent a variety of metrics, such as wattage, optical resolution, etc. The "satellite size scaling" by mass m_o represents a simply way to account for the power of satellite j relative to a nominal satellite represented by m_o. This expression also accounts for degradation of the signal ($S_{i/j}^g \leq S_o$) is the satellite is not directly ($\boldsymbol{r}_j^s \neq \boldsymbol{r}_i^g$) overhead ("overhead scaling"). This model accounts for basic trends and could be enhanced if a "library" of specific satellite types were introduced. The projection onto the surface normal at ground site i, and the relative position vector ($\boldsymbol{r}_j^s - \boldsymbol{r}_i^g$) between the satellite j and the ground position i (Fig. 7) is given by

$$I_{i/j} = (\boldsymbol{r}_j^s - \boldsymbol{r}_i^g) \cdot \boldsymbol{n}_i^g \tag{3.2}$$

- The *total* signal strength from all satellites $j = 1, 2, \ldots N^s$

$$S_i^{g,tot} = \sum_{j=1}^{N^s} S_{i/j}^g. \tag{3.3}$$

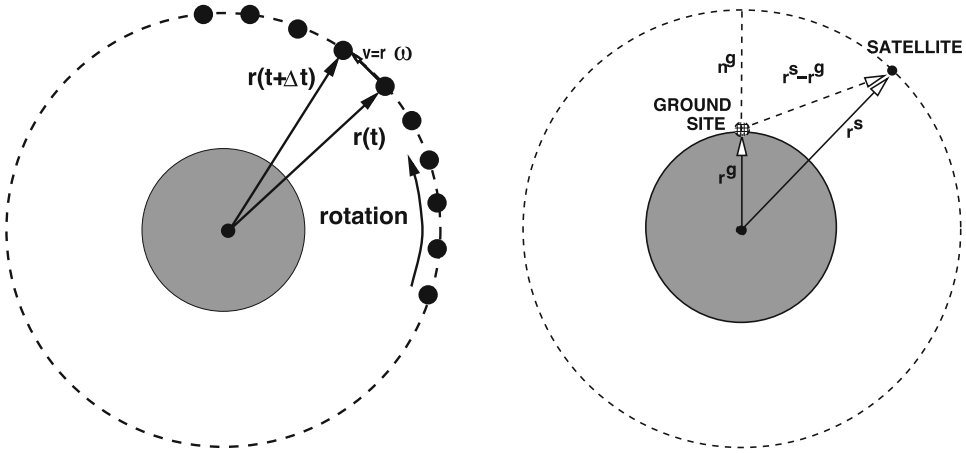

Fig. 7 Left: Steady-state circular orbit calculation. Right: The relative position vectors for the performance metric calculations

- The average error in the signal received for all of the sites at a given moment in time

$$E^{g,tot,ave}(t) = \sqrt{\sum_{i=1}^{N^g} \left(\frac{S_i^{g,tot}(t) - S^{g,target}}{S^{g,target}} \right)^2}. \quad (3.4)$$

- The total time simulation error average

$$\langle E^{g,tot,ave}(t) \rangle_T = \frac{1}{T} \int_0^T E^{g,tot,ave}(t)\, dt \stackrel{\text{def}}{=} \Pi^{(s)}, \quad (3.5)$$

where $\Pi^{(s)}$ is a cost function.

- A cost for the satellite number:

$$1 \geq \Pi^{N^s} \stackrel{\text{def}}{=} \frac{\Delta N_s - 1}{\Delta N^{s,max} - 1} \geq 0, \quad (3.6)$$

- A cost for the satellite orbital radii:

$$1 \geq \Pi^{r^s} \stackrel{\text{def}}{=} \frac{\Delta r_s - 1}{\Delta r^{s,max} - 1} \geq 0, \quad (3.7)$$

- A cost for the satellite orbital speeds:

$$1 \geq \Pi^{\omega^s} \stackrel{\text{def}}{=} \frac{\Delta \omega_s - 1}{\Delta \omega^{s,max} - 1} \geq 0 \quad (3.8)$$

and

- A cost for the satellite sizes:

$$1 \geq \Pi^{L^s} \stackrel{\text{def}}{=} \frac{\Delta L_s - 1}{\Delta L^{s,max} - 1} \geq 0. \quad (3.9)$$

Figure 8 illustrates the results for a sequence of the orbital performance. Shown on the surface of Planet-X are the signal strengths received from all of the satellites.

- **STEP 4**: Constellation Performance: With these quantities in hand, one can construct the total cost function:

$$\Pi(\mathbf{\Lambda}) = \frac{1}{\sum_{i=1}^{5} w_i} \left(\underbrace{w_1 \Pi^{(S)}}_{\text{signal cost}} + \underbrace{w_2 \Pi^{N^s}}_{\text{satellite cost}} + \underbrace{w_3 \Pi^{r^s}}_{\text{orbit cost}} + \underbrace{w_4 \Pi^{\omega^s}}_{\text{speed cost}} + \underbrace{w_5 \Pi^{L^s}}_{\text{size cost}} \right) \quad (3.10)$$

where $\mathbf{\Lambda} = (\Lambda_1, \ldots, \Lambda_N)$ is the design vector of system parameters and the weights are $0 \leq w_1, w_2, w_3, w_4, w_5 \leq 1$, each of which indicate the relative importance of the particular objective.

4 System parameter search: machine learning algorithm (MLA)

The rapid speed at which these simulations are completed gives researchers the ability to explore inverse problems seeking to determine the parameter combinations that can deliver the smallest cost function. In order to cast the objective mathematically, we set up an inverse problem as a Machine Learning Algorithm (MLA); specifically a Genetic MLA (G-MLA) variant, which is well-suited for nonconvex optimization. Following Zohdi [57–65], we formulate the objective as a cost function minimization problem that seeks system parameters to match a desired response, by minimizing $\Pi(\mathbf{\Lambda})$ in Eq. (3.10), by varying the design parameter sets $(i = 1, 2, ...,)$

$$\mathbf{\Lambda}^i \stackrel{\text{def}}{=} \{\Lambda_1^i, \Lambda_2^i, \Lambda_3^i, \ldots, \Lambda_N^i\}. \quad (4.1)$$

The system parameter search is conducted within the constrained ranges $\Lambda_1^{(-)} \leq \Lambda_1 \leq \Lambda_1^{(+)}$, $\Lambda_2^{(-)} \leq \Lambda_2 \leq \Lambda_2^{(+)}$ and $\Lambda_3^{(-)} \leq \Lambda_3 \leq \Lambda_3^{(+)}$, etc. These upper and lower limits

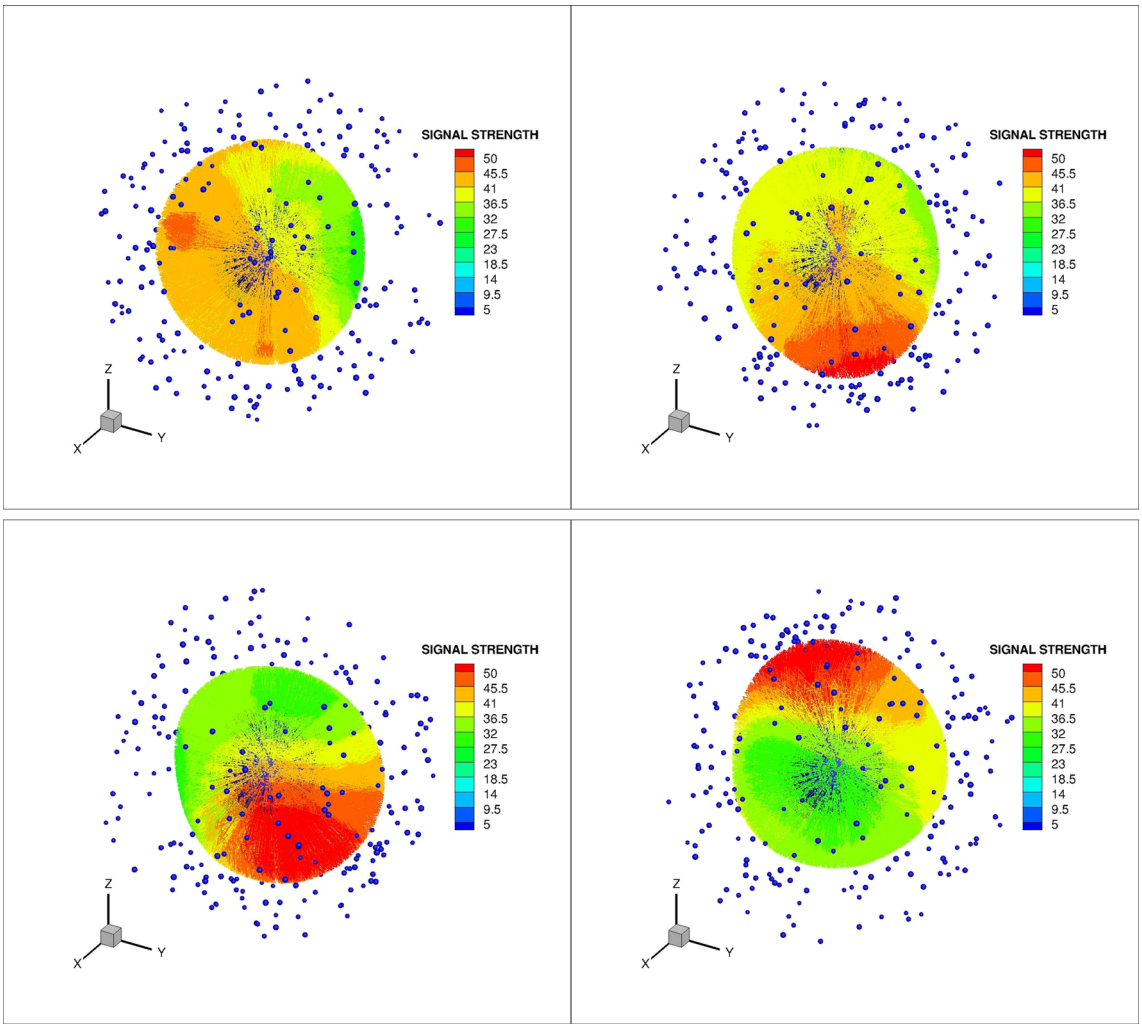

Fig. 8 A sequence of the orbital performance. Shown on the surface of Planet X are the signal strengths received from all of the satellites

would, in general, be dictated by what is physically feasible (Fig. 9).

4.1 Algorithmic details

Here we follow Zohdi [57–65] in order to minimize Eq. (3.10), which we will refer to as the composite "cost function". Cost functions such as Eq. (3.10) are nonconvex in design parameter space and often nonsmooth. Their minimization is usually difficult with direct application of gradient methods. This motivates derivative-free search methods, for example those found in Machine Learning Algorithms (MLAs). One of the most basic subsets of MLAs are so-called Genetic Algorithms (GAs), or as we refer to them in this work, Genetic MLA (G-MLA). Typically, one will use a GA first in order to isolate multiple local minima, and then use a gradient-based algorithm in these locally convex regions or reset the GA to concentrate its search over these more constrained regions. GAs are typically the simplest scheme to start the analysis, and one can, of course, use more sophisticated methods if warranted. For a review of GAs, see the pioneering work of Holland [66, 67], as well as Goldberg [68], Davis [69], Onwubiko [70] and Goldberg and Deb [71].

4.2 Generalities

The MLA/GA approach is extremely well-suited for nonconvex, nonsmooth, multicomponent, multistage systems and, broadly speaking, involves the following essential concepts:

1. *POPULATION GENERATION:* Generate a parameter population of genetic strings: $\mathbf{\Lambda}^i$.
2. *PERFORMANCE EVALUATION:* Compute performance of each genetic string: $\Pi(\mathbf{\Lambda}^i)$.
3. *RANK STRINGS:* Rank them $\mathbf{\Lambda}^i$, $i = 1, \ldots, S$.
4. *MATING PROCESS:* Mate pairs/produce offspring.
5. *GENE ELIMINATION:* Eliminate poorly performing genetic strings.

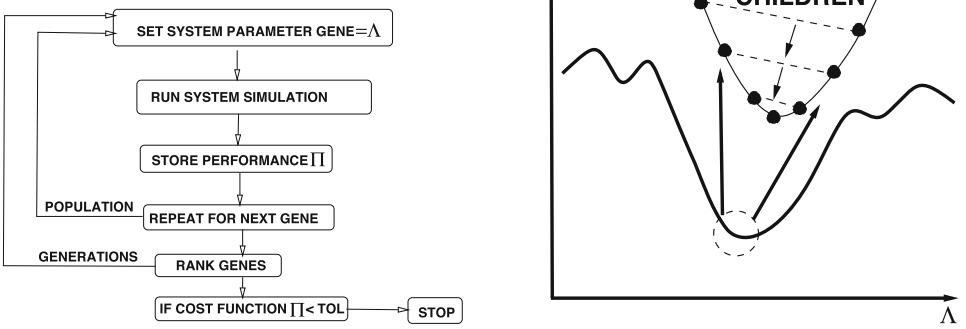

Fig. 9 The basic action of the Genetic MLA (G-MLA, Zohdi [57–65])

6. *POPULATION REGENERATION:* Repeat process with updated gene pool and new *random* genetic strings.
7. *SOLUTION POST-PROCESSING:* Employ gradient-based methods afterwards in local "valleys", *if smooth enough*.

4.3 Specifics

Following Zohdi [57–65] the algorithm is as follows:

- **STEP 1**: Randomly generate a population of S starting genetic strings, $\mathbf{\Lambda}^i$, $(i = 1, 2, 3, \ldots, S)$:

$$\mathbf{\Lambda} i \stackrel{\text{def}}{=} \left\{ \begin{array}{c} \Lambda i_1 \\ \Lambda i_2 \\ \Lambda i_3 \\ \ldots \\ \Lambda i_N \end{array} \right\} \tag{4.2}$$

- **STEP 2**: Compute fitness of each string $\Pi(\mathbf{\Lambda}^i)$, (i=1,…, S)
- **STEP 3**: Rank genetic strings: $\mathbf{\Lambda}^i$, (i=1,…, S)
- **STEP 4**: Mate nearest pairs and produce two offspring, (i=1,…, S):

$$\boldsymbol{\lambda}^i \stackrel{\text{def}}{=} \mathbf{\Phi} \circ \mathbf{\Lambda}^i + (\mathbf{1} - \mathbf{\Phi}) \circ \mathbf{\Lambda}^{\mathbf{i+1}} \stackrel{\text{def}}{=} \left\{ \begin{array}{c} \phi_1 \Lambda_1^i \\ \phi_2 \Lambda_2^i \\ \phi_3 \Lambda_3^i \\ \ldots \\ \phi_N \Lambda i_N \end{array} \right\} + \left\{ \begin{array}{c} (1-\phi_1)\Lambda_1^{i+1} \\ (1-\phi_2)\Lambda_2^{i+1} \\ (1-\phi_3)\Lambda_3^{i+1} \\ \ldots \\ (1-\phi_N)\Lambda_N^{i+1} \end{array} \right\} \tag{4.3}$$

and

$$\boldsymbol{\lambda}^{i+1} \stackrel{\text{def}}{=} \mathbf{\Gamma} \circ \mathbf{\Lambda}^i + (\mathbf{1} - \mathbf{\Gamma}) \circ \mathbf{\Lambda}^{\mathbf{i+1}} \stackrel{\text{def}}{=} \left\{ \begin{array}{c} \gamma_1 \Lambda_1^i \\ \gamma_2 \Lambda_2^i \\ \gamma_3 \Lambda_3^i \\ \ldots \\ \gamma_N \Lambda_N \end{array} \right\} + \left\{ \begin{array}{c} (1-\gamma_1)\Lambda_1^{i+1} \\ (1-\gamma_2)\Lambda_2^{i+1} \\ (1-\gamma_3)\Lambda_3^{i+1} \\ \ldots \\ (1-\gamma_N)\Lambda_N^{i+1} \end{array} \right\} \tag{4.4}$$

where for this operation, the ϕ_i and γ_i are random numbers, such that $0 \leq \phi_i \leq 1$, $0 \leq \gamma_i \leq 1$, which are different for each component of each genetic string.

- **STEP 5**: Eliminate the worst performing M strings and keep top K parents and their K offspring (K offspring+K parents+M=S).
- **STEP 6**: Repeat STEPS 1–6 with top gene pool (K offspring and K parents), plus M new, randomly generated, strings.
- **IMPORTANT OPTION**: Rescale and restart the search around best performing parameter set every few generations

Remark 1 If one selects the mating parameter Φ to be greater than one and/or less than zero, one can induce "mutations", i.e. characteristics that neither parent possesses. However, this is somewhat redundant with introduction of new random members of the population in the current algorithm.

Remark 2 If one does not retain the parents in the algorithm above, it is possible that inferior performing offspring may replace superior parents. Thus, top parents should be kept for the next generation. This guarantees a monotone reduction in the cost function. Furthermore, retained parents do not need to be ranked or reevaluated, making the algorithm less computationally expensive. Numerous studies by the author have shown that the advantages of parent retention outweighs

inbreeding, for sufficiently large population sizes. Also, we note that this algorithm is easily parallelizable.

Remark 3 After application of such a global search algorithm, one can apply a gradient-based method, if the cost function is sufficiently smooth in that region of the parameter space. In other words, if one has located a convex portion of the parameter space with a global genetic search, one can employ gradient-based procedures locally to minimize the objective function further, since they are generally much more efficient for convex optimization of smooth functions. An exhaustive review of these methods can be found in the texts of Luenberger [72] and Gill, Murray and Wright [73].

5 Model problem

The system was optimized (Eq. 3.10) varying the following four parameters (and ranges) introduced earlier:

- Satellite number: $N_o^s \leq N_j^s \leq N^{s,max}$, where $N_j^s = N_o^s + (N^{s,max} - N_o^s) \times RAND_j$,
- Satellite orbital radii: $r_o^s \leq r_j^s \leq r_o^s \times (1 + (\Delta r^s - 1) \times RAND_j)$, where $1 \leq \Delta r^s \leq \Delta r^{s,max}$,
- Satellite orbital speeds: $\omega_o^s \leq \omega_j^s \leq \omega_o^s \times (1 + (\Delta \omega^s - 1) \times RAND_j)$, where $1 \leq \Delta \omega^s \leq \Delta \omega^{s,max}$ and
- Satellite sizes: $L_o^s \leq L_j^s \leq L_o^s \times (1 + (\Delta L^s - 1) \times RAND_j)$, where $1 \leq \Delta L^s \leq \Delta L^{s,max}$.

The desired target values were:

- The desired target average received signal: $\langle S^{g,tot,des} \rangle_T = 20$.
- Satellite number (the lower bound): N_o^s,
- Satellite orbital radii (the lower bound): r_o^s,
- Satellite orbital speeds (the lower bound): ω_o^s and
- Satellite sizes (the lower bound): L_o^s.

6 Tests with variations in weights

The design parameters $\mathbf{\Lambda} = \{\Lambda_1, \Lambda_2 \ldots \Lambda_N\}$ were optimized over the search intervals (4 variables): $\mathbf{\Lambda}_i^- \leq \mathbf{\Lambda}_i \leq \mathbf{\Lambda}_i^+, i = 1, 2, \ldots 4$. We used the following MLA settings:

- Number of design variables: 4,
- Population size per generation: 24,
- Number of parents to keep in each generation: 6,
- Number of children created in each generation: 6,
- Number of completely new genes created in each generation: 12,
- Number of generations for re-adaptation around a new search interval: 10 and
- Number of generations: 100.

The algorithm was automatically reset around the best gene every 10 generations. The entire 100 generation simulation, with 24 genes per evaluation (2400 total designs) took a few minutes on a laptop, *making it ideal as a design tool.* We note that, for a given set of parameters, each complete simulation takes on the order of 0.1 s, several thousand parameter sets can be evaluated in well under an hour, *without even exploiting the inherent parallelism of the MLA/GA.*

Figure 10 shows the reduction of the cost function (Eq. 3.10) for the four parameter set for various weighted objectives. Shown is the performance of the best performing gene (*red*) as a function of successive generations, as well as the average performance of the entire population (*green*). Table 1 and Fig. 10 illustrate the results. The trends are as follows:

- As Cases 2–6 $\{w_1 = 1, w_2, w_3, w_4, w_5\}$ indicate, as $w_i \to 1$, for $i = 2, 3, 4, 5$, the tradeoff between Planet-X coverage and satellite constellation infrastructural cost becomes apparent.
- For Case 1 $\{1, 0, 0, 0, 0\}$, where there is no weighted consideration for constellation infrastructural costs, the best satellite constellation infrastructural design required 141 satellites with a relatively large orbital spread, allowing for more coverage for single satellite in larger orbits. The orbital speed and satellite size were not particularly important variables.
- For Cases 2–6 $\{w_1 = 1, w_2, w_3, w_4, w_5\}$, as $w_i \to 1$, for $i = 2, 3, 4, 5$, the infrastructural costs of having larger orbits begins to dominate, leading the algorithm to push for lower orbits, which requires more satellites to attempt to meet the coverage and a corresponding tradeoff between global signal coverage over Planet-X's surface and constellation cost.

7 Summary and extensions

This work developed a digital-twin framework for a constellation of satellites. The fast simulation speed allows one to explore inverse problems that seek parameter combinations, represented by a multicomponent vector of comprised of

- Satellite number,
- Satellite orbital shells,
- Satellite orbital speeds and
- Satellite sizes,

which can deliver desired system performance. In order to cast the objective mathematically, we set up an inverse problem as a Machine Learning Algorithm (MLA); specifically a Genetic MLA (G-MLA) variant, which is well-suited for

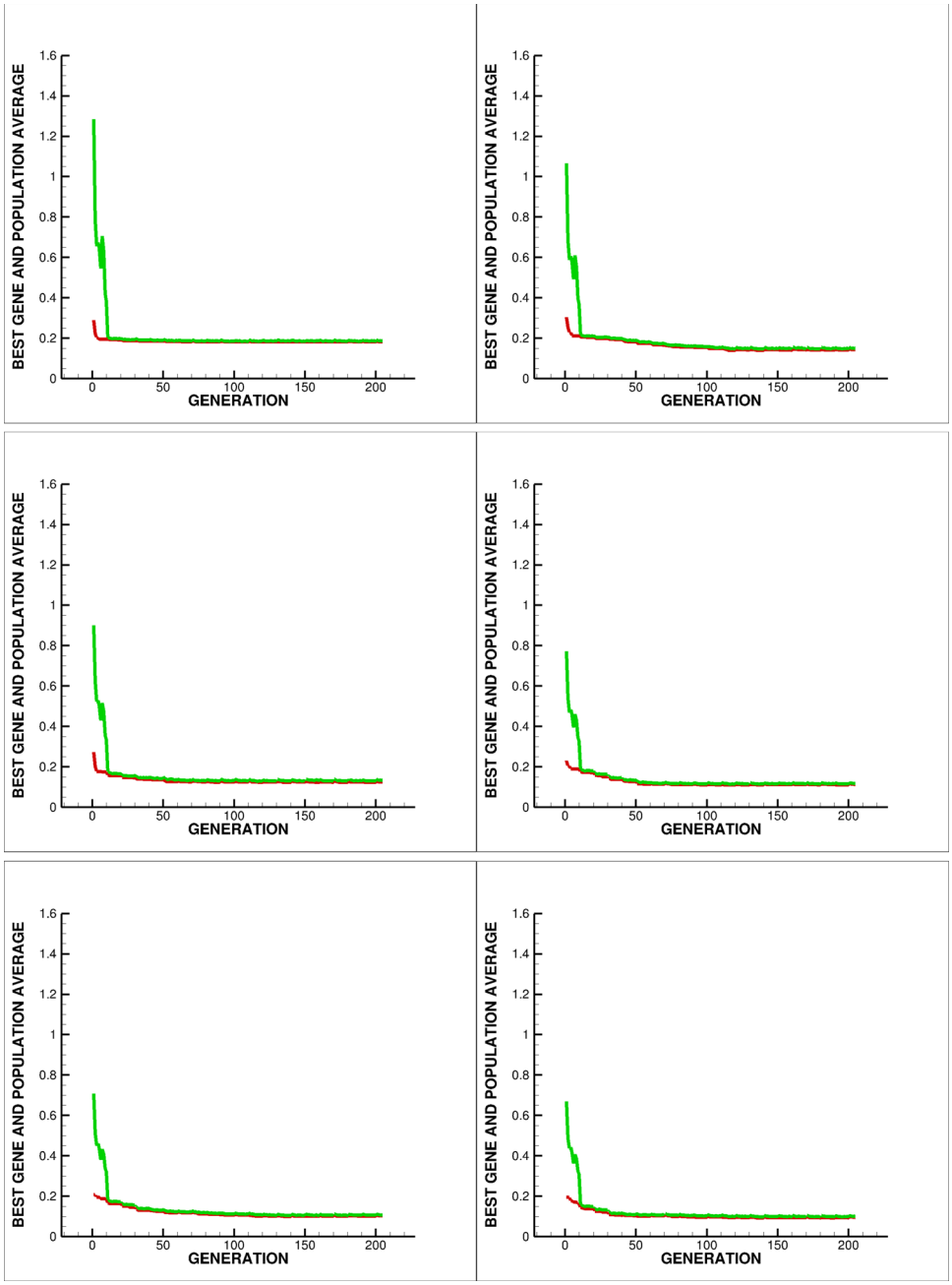

Fig. 10 Left: The red plot is the cost function associated with the best performing gene and the green function is the average cost function of the entire population. In all cases, the minimization stabilized between 150–200 generations. Top left to right and top to bottom: $\{w_1, w_2, w_3, w_4, w_5\} =$ {1, 0, 0, 0, 0}, {1, 0.1, 0.1, 0.1, 0.1}, {1, 0.25, 0.25, 0.25, 0.25}, {1, 0.5, 0.5, 0.5, 0.5}, {1, 0.75, 0.75, 0.75, 0.75}, {1, 1, 1, 1, 1}

nonconvex optimization. Numerical examples were provided to illustrate the framework. The extensions to such an analysis are wide ranging, in particular including more complex, noncircular orbits and transfer maneuvers between orbital shells. As was mentioned in the body of the work, the simplified cost function represents (1) the proper coverage of the planet by the constellation and (2) the expense of deploying and maintaining the constellation. While characterizing the coverage of the planet is relatively straightforward, since it is essentially geometric (Fig. 3), the costs associated with the expense of deploying and maintaining the constellation were simplified, using the following general trends:

- More satellites make the system more expensive to manufacture and to manage in orbit,
- Larger orbits provide better coverage, but are more expensive, due to launch power needed for larger orbits,
- Faster traveling satellites are more expensive, due to the power needed to maintain faster orbital speeds,
- Larger satellites provide better coverage, but are more expensive, due to launch power needed and more power needed to operate and maintain them in orbit.

These are clearly generalized simplifications, since there is potentially significant coupling between these trends. Fur-

Table 1 The top system parameter performers ($\mathbf{\Lambda}_1 - \mathbf{\Lambda}_4$) for different weight vectors

$\{w_1, w_2, w_3, w_4, w_5\}$	$\mathbf{\Lambda}_1 = N^s$	$\mathbf{\Lambda}_2 = \Delta r^s$	$\mathbf{\Lambda}_3 = \Delta\omega^s$	$\mathbf{\Lambda}_4 = \Delta L^s$	$\Pi^{\omega t}$	Π^S	Π^{N^s}	Π^{r^s}	Π^{ω^s}	Π^{L^s}
{1.00, 0.00, 0.00, 0.00, 0.00}	141	1.7560	1.1114	1.0183	0.1820	0.1820	0.1366	0.7560	0.1114	0.0183
{1.00, 0.10, 0.10, 0.10, 0.10}	195	1.0102	1.0239	1.0156	0.1434	0.1868	0.3433	0.0294	0.0072	0.0036
{1.00, 0.25, 0.25, 0.25, 0.25}	195	1.0075	1.0183	1.0098	0.1259	0.1637	0.3166	0.0075	0.0183	0.0098
{1.00, 0.50, 0.50, 0.50, 0.50}	173	1.0172	1.0021	1.0089	0.1131	0.2036	0.2433	0.0172	0.0021	0.0089
{1.00, 0.75, 0.75, 0.75, 0.75}	166	1.0112	1.0078	1.0085	0.1023	0.2235	0.2200	0.0112	0.0078	0.0085
{1.00, 1.00, 1.00, 1.00, 1.00}	159	1.0120	1.0073	1.0074	0.0946	0.2529	0.1933	0.0120	0.0073	0.0074

thermore, there is an expense in maintaining a circular orbit at a certain speed (see Eq. 1.1), requiring the calculation of the energy needed for each satellite, W_j, $j = 1, 2, \ldots, N^s$

$$W_j = \int_0^T \boldsymbol{F}_j^{other}(t) \cdot \boldsymbol{v}_j \, dt, \tag{7.1}$$

using the general Eqs. (2.10)–(2.15). Depending on the type of satellite, one could also incorporate the possibility of solar recharging. As indicated, more detailed analysis would need to focus on the specific type of satellites deployed, which is outside the scope of the current work, but which is being pursued by the author. Further extensions to this analysis for general satellite dynamics should include non-circular orbits and energetic costs of inter-orbital transfers, such as the Hohmann Transfer [74] process, whereby one (1) makes direct ascent to a low parking altitude and (2) transfers to a higher circular orbit by means of an elliptical transfer orbit which is tangent to both circular orbits. Accordingly, in closing, we outline some general orbital characteristics that emanate from the orbital trajectory equation.

7.1 General orbital trajectories

The conservation of angular momentum will be useful in further orbital analysis. From a freebody diagram of the satellite, in the absence of thrust, the position vector $\boldsymbol{r}$ and the force $\boldsymbol{F}$ are collinear, thus (Fig. 4)

$$\frac{d}{dt}\boldsymbol{H}_o = \boldsymbol{M}_o = \boldsymbol{r} \times \boldsymbol{F} = \boldsymbol{0} \Rightarrow \boldsymbol{H_o} = \boldsymbol{r} \times \mathbf{m}\boldsymbol{v} = \textbf{constant}, \tag{7.2}$$

where $\boldsymbol{H}_o$ is the angular momentum around the planet center (o) and $\boldsymbol{M}_o$ is the the sum of external moments in the system, which is a form of the statement of conservation of angular momentum. Thus, for any two locations (a) and (p) in orbit (Fig. 11)

$$\boldsymbol{H}_o(\boldsymbol{r}_a) = \boldsymbol{r}_a \times m\boldsymbol{v}_a = \boldsymbol{r}_p \times m\boldsymbol{v}_p = \boldsymbol{H}_o(\boldsymbol{r}_p). \tag{7.3}$$

A particularly useful quantity is the specific angular momentum $\boldsymbol{h} = \boldsymbol{r} \times \boldsymbol{v} = \frac{\boldsymbol{H}}{m}$, which helps with the solution to the trajectory equation, introduced earlier

$$m_j \ddot{\boldsymbol{r}}_j + \frac{GM_{px}m_j}{r_j^3}\boldsymbol{r}_j = \boldsymbol{0} \Rightarrow \ddot{\boldsymbol{r}}_j + \frac{\mu_{px}}{r_j^3}\boldsymbol{r}_j = \boldsymbol{0}, \tag{7.4}$$

where $\mu_{px} = GM_{px}$. Let us again consider a single satellite, $j = 1$, thus eliminating the need for subscripts $j = 1, 2, \ldots, N^s$. Following Bate et al. [75] as a guide

$$\ddot{\boldsymbol{r}} + \frac{\mu_{px}}{r^3}\boldsymbol{r} = \boldsymbol{0} \Rightarrow \ddot{\boldsymbol{r}} = -\frac{\mu_{px}}{r^3}\boldsymbol{r}, \tag{7.5}$$

and taking the cross-products of both sides with $\boldsymbol{h}$, yields

$$\begin{aligned}\mu_{px}\ddot{\boldsymbol{r}} \times \boldsymbol{h} &= -\frac{\mu_{px}}{r^3}\boldsymbol{r} \times \boldsymbol{h} \\ &= \boldsymbol{h} \times \frac{\mu_{px}}{r^3}\boldsymbol{r} \\ &= \frac{\mu_{px}}{r^3}(\boldsymbol{r} \times \boldsymbol{v}) \times \boldsymbol{r} \\ &= \frac{\mu_{px}}{r^3}(\boldsymbol{v}(\boldsymbol{r} \cdot \boldsymbol{r}) - \boldsymbol{r}(\boldsymbol{r} \cdot \boldsymbol{v})) \\ &= \frac{\mu_{px}}{r}\boldsymbol{v} - \mu_{px}\frac{\dot{r}}{r^2}\boldsymbol{r}, \end{aligned} \tag{7.6}$$

where $\boldsymbol{r} \cdot \dot{\boldsymbol{r}} = ||\boldsymbol{r}||||\dot{\boldsymbol{r}}||$, since $\boldsymbol{r}$ and $\dot{\boldsymbol{r}}$ are collinear. Also noting that

$$\mu_{px}\frac{d}{dt}\left(\frac{\boldsymbol{r}}{r}\right) = \frac{\mu_{px}}{r}\boldsymbol{v} - \mu_{px}\frac{\dot{r}}{r^2}\boldsymbol{r}, \tag{7.7}$$

and

$$\frac{d}{dt}(\dot{\boldsymbol{r}} \times \boldsymbol{h}) = \ddot{\boldsymbol{r}} \times \boldsymbol{h} + \dot{\boldsymbol{r}} \times \frac{d\boldsymbol{h}}{dt} = \ddot{\boldsymbol{r}} \times \boldsymbol{h} + \boldsymbol{0}, \tag{7.8}$$

yields, from Eq. (7.6)

$$\frac{d}{dt}(\dot{\boldsymbol{r}} \times \boldsymbol{h}) = \mu_{px}\frac{d}{dt}\left(\frac{\boldsymbol{r}}{r}\right). \tag{7.9}$$

Integrating both sides leads to

$$\dot{\boldsymbol{r}} \times \boldsymbol{h} = \mu_{px}\frac{\boldsymbol{r}}{r} + \boldsymbol{K}, \tag{7.10}$$

where $\boldsymbol{K}$ is a vector constant of integration. Taking the dot product with $\boldsymbol{r}$ on either side

$$\boldsymbol{r} \cdot (\dot{\boldsymbol{r}} \times \boldsymbol{h}) = \boldsymbol{r} \cdot \left(\mu_{px}\frac{\boldsymbol{r}}{r} + \boldsymbol{K}\right) \tag{7.11}$$

and utilizing the vector identity, $\boldsymbol{a} \cdot (\boldsymbol{b} \times \boldsymbol{c}) = \boldsymbol{c} \cdot (\boldsymbol{a} \times \boldsymbol{b})$ yields ($h = ||\boldsymbol{h}||$ and $K = ||\boldsymbol{K}||$) leads to

$$h^2 = \mu_{px}r + rK\cos\theta \tag{7.12}$$

and thus

$$r = \frac{\frac{h^2}{\mu_{px}}}{1 + \frac{K}{\mu_{px}}\cos\theta} = \frac{p}{1 + e\cos\theta}, \tag{7.13}$$

where p is known as the trajectory parameter and e is the eccentricity.

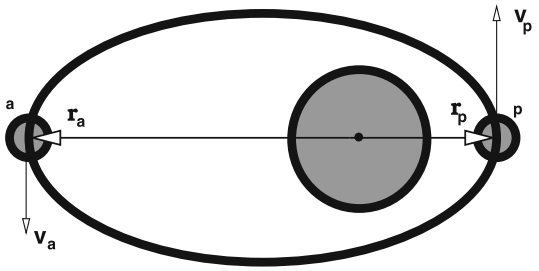

Fig. 11 Points during orbit: p = periapsis (minimum radius) and a = apoapsis (maximum radiius)

7.2 Conic sections and orbits

Equation (7.13) describes conic sections (Fig. 12)

$$r = \frac{p}{1 + e\cos\theta}, \tag{7.14}$$

where $e = \frac{c}{a}$ and $p = a(1 - e^2)$ (except for a parabola):

- $e = 0$ is a circle,
- $0 < e < 1$ is an ellipse,
- $e = 1$ is a parabola and
- $e > 1$ is a hyperbola.

The minimum orbital radius, known as periapsis, is

$$r_{min} = \frac{p}{1 + ecos(0)} = a(1 - e) \tag{7.15}$$

and the maximum, known as apoapsis, is

$$r_{max} = \frac{p}{1 + ecos(\pi)} = a(1 + e). \tag{7.16}$$

Utilizing, $p = \frac{h^2}{\mu_{px}}$ and defining the specific potential energy (E), one can show (for example see Bate et al. [75])

$$\begin{aligned} E &= \frac{1}{2}\boldsymbol{v} \cdot \boldsymbol{v} - \frac{\mu_{px}}{r} = \frac{h^2}{2r_p^2} - \frac{\mu_{px}}{r_p} \\ &= \frac{\mu_{px}a(1 - e^2)}{2a^2(1 - e)^2} - \frac{\mu_{px}}{a(1 - e)} = -\frac{\mu_{px}}{2a}. \end{aligned} \tag{7.17}$$

Thus

$$p = a(1 - e^2) = \frac{h^2}{\mu_{px}} \Rightarrow e = \left(1 - \frac{p}{a}\right)^{1/2} \quad \text{and}$$
$$a = -\frac{\mu_{px}}{2E}, \tag{7.18}$$

and for any conic section

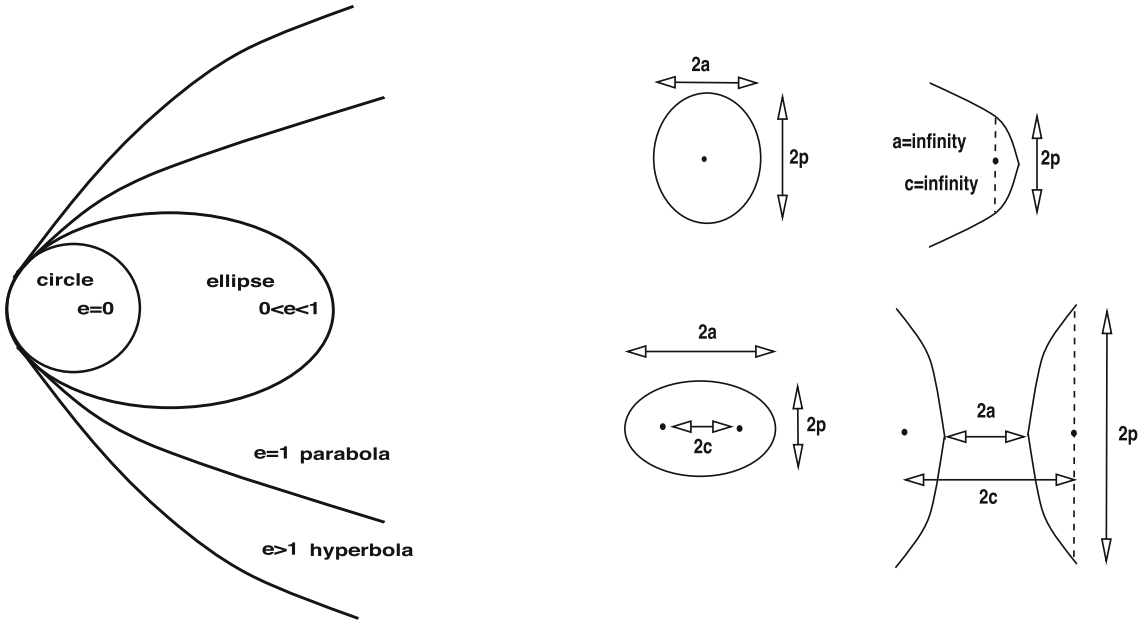

Fig. 12 Conic sections which describe various orbits

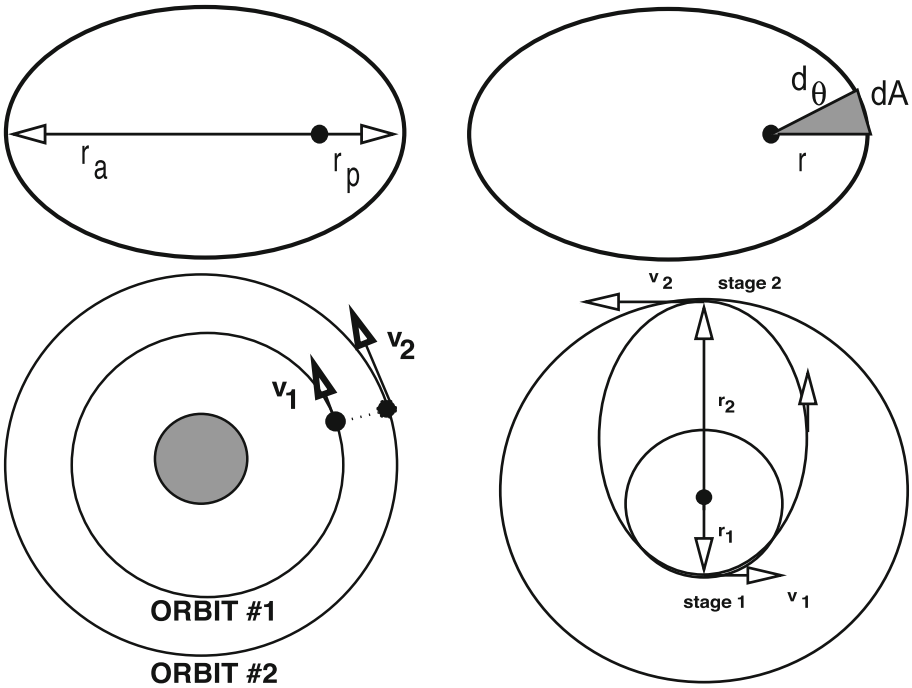

Fig. 13 Differential area of an elliptical orbit

Fig. 14 Orbital changes and the Hohmann [74] transfer orbit process

$$e = \left(1 + \frac{2Eh^2}{\mu_{px}^2}\right)^{1/2}. \tag{7.19}$$

If $E < 0$ then the orbit is a circle or ellipse, if $E = 0$ the satellite has achieved escape velocity and if $E > 0$ the orbit is a parabola or hyperbola. The eccentricity can also be characterized as

$$e = \frac{r_a - r_p}{r_a + r_p}. \tag{7.20}$$

The angular momentum is

$$h = r^2 \frac{d\theta}{dt} \Rightarrow dt = \frac{r^2}{h} d\theta \Rightarrow dA = \frac{1}{2} r^2 d\theta \tag{7.21}$$

and (Fig. 13)

$$dt = \frac{r^2}{h}d\theta = \frac{2}{h}dA \Rightarrow \int_0^T dt = \int_o^A \frac{2}{h}dA, \tag{7.22}$$

thus, the period is

$$T^p = \frac{2\pi ab}{h}. \tag{7.23}$$

Also, since $b = \sqrt{a^2 - c^2} = \sqrt{a^2(1-e^2)} = \sqrt{ap}$ and $h = \sqrt{\mu_{px}p}$, thus

$$T^p = \frac{2\pi}{\mu_{px}^{1/2}}a^{3/2}. \tag{7.24}$$

In the special case that $a = b$, a circular orbit arises and

$$T^p = \frac{2\pi}{\mu_{px}^{1/2}}r_c^{3/2}. \tag{7.25}$$

For circular orbits

$$E = -\frac{\mu_{px}}{2r_c} = \frac{v^2}{2} - \frac{\mu_{px}}{r_c} \Rightarrow v_c = \left(\frac{\mu_{px}}{r_c}\right)^{1/2}, \tag{7.26}$$

or, equivalently, from a freebody diagram

$$m\frac{v^2}{r} = \frac{GM_{px}m}{r^2} \Rightarrow v_c = \left(\frac{\mu_{px}}{r_c}\right)^{1/2}, \tag{7.27}$$

which is equivalent to Eq. (1.1).

7.3 Changes in orbits

A relatively straightforward way to characterize the cost of changing from one orbit to another, is from a basic work-energy principle. For an object in stable (drag-free, loss-less) orbit the total potential energy is constant (system energy input $\Delta W_{a\to b} = 0$)

$$\underbrace{\left(\frac{1}{2}m\boldsymbol{v}\cdot\boldsymbol{v} - \frac{GM_{px}m}{r}\right)}_{orbit\ point\ a} + \underbrace{\Delta W_{a\to b}}_{for\ a\ loss\text{-}less\ orbit=0}$$
$$= \underbrace{\left(\frac{1}{2}m\boldsymbol{v}\cdot\boldsymbol{v} - \frac{GM_{px}m}{r}\right)}_{orbit\ point\ b} = constant, \tag{7.28}$$

where m is the mass of the satellite and M_{px} is the mass of the planet and r_{px} is the radius between them.[1] However, for orbital changes (Fig. 14), a cost is incurred, namely incremental energy $\Delta W_{O_1\to O_2} \neq 0$

$$\underbrace{\left(\frac{1}{2}m\boldsymbol{v}\cdot\boldsymbol{v} - \frac{GM_{px}m}{r}\right)}_{Orbit\#1} + \underbrace{\Delta W_{O_1\to O_2}}_{\neq 0}$$
$$= \underbrace{\left(\frac{1}{2}m\boldsymbol{v}\cdot\boldsymbol{v} - \frac{GM_{px}m}{r}\right)}_{Orbit\#2}. \tag{7.30}$$

As mentioned in the body of the work, there are economical ways to induce in-plane orbital changes, such as the so-called "Hohmann Transfer" [74], which is an energy-efficient way to shift from one circular orbit to another coplanar orbit by (Fig. 14),

- Making direct ascent to a circular low altitude parking orbit and
- Transferring to a higher circular orbit by means of an intermediate elliptical transfer orbit which is tangent to both circular orbits,

specifically by following these three steps:

- Step 1: Place the satellite in a circular "parking orbit",
- Step 2: Pulse (thrust) at a key position yielding a temporarily elliptical "transfer orbit" and
- Step 3: Pulse at another key position yielding a permanent circular orbit.

This process is extremely energy-efficient, but takes longer than more complex aggressive thrust-control processes-such precise adaptive feedback control processes, which require numerical methods to ascertain guidance. For extensive details, we refer the reader to the classical treatise of Bate et al. [75]. There are even more energy-efficient methods designed for interplanetary navigation, known as the Interplanetary Transport Network (ITN), utilizing gravity-assist from planet to planet, for which we refer the reader to Lo and Ross [76] for more details. The incorporation of more complex (non-circular) orbital configurations and inclusion of adaptive feedback control maneuvers in the overall digital-twin model are the subject of current research by the author.

[1] From this, one can ascertain the "escape" velocity for a non-propelled object to escape gravitational pull by setting the second-state velocity to be zero and the radius to be infinity:

$$\underbrace{\left(\frac{1}{2}m\boldsymbol{v}^e\cdot\boldsymbol{v}^e - \frac{GM_{px}m}{r_{px}}\right)}_{launch} = \underbrace{0+0}_{second\ state} \Rightarrow v^e = \left(\frac{2GM_{px}}{r_{px}}\right)^{1/2}. \tag{7.29}$$

With Earth's parameters, $M_{px} = M_e$ and $r_{px} = r_e$, this corresponds to $v^e \approx 11{,}200$ m/s.

Acknowledgements This work has been supported by the UC Berkeley College of Engineering.

Declarations

Conflict of interest The author states that there is no conflict of interest.

References

1. Walker JG (1982) Comments on Rosette constellations of earth satellites. IEEE Trans Aerosp Electron Syst 18(4):723–724
2. Walker JG (1984) Satellite constellations. J Br Interplanet Soc 37:559–571
3. Curzi G, Modenini D, Tortora P (2020) Large constellations of small satellites: a survey of near future challenges and missions. Aerospace 7:133. https://doi.org/10.3390/aerospace7090133
4. Ballard AH (1980) Rosette constellations of earth satellites. IEEE Trans Aerosp Electron Syst 16(5)
5. del Portillo I, Cameron BG, Crawley EF (2019) A technical comparison of three low earth orbit satellite constellation systems to provide global broadband. Acta Astronautica 159:123–135. Bibcode:2019AcAau.159..123D. https://doi.org/10.1016/j.actaastro.2019.03.040. hdl:1721.1/135044.2. ISSN 0094-5765. S2CID 115993580
6. Bhattacherjee D, Singla A(2019) Network topology design at 27,000 km/hour. In: Proceedings of the 15th international conference on emerging networking experiments and technologies. CoNEXT'19. Association for Computing Machinery, Orlando, pp 341–354. https://doi.org/10.1145/3359989.3365407. ISBN 978-1-4503-6998-5. S2CID 208946393
7. Bhattacherjee D, Aqeel W, Bozkurt IN, Aguirre A, Chandrasekaran B, Godfrey PB, Laughlin G, Maggs B, Singla A (2018) Gearing up for the 21st century space race. In: Proceedings of the 17th ACM workshop on hot topics in networks. HotNets'18. Association for Computing Machinery, Redmond, pp 113–119. https://doi.org/10.1145/3286062.3286079. ISBN 978-1-4503-6120-0
8. Handley M (2018) Delay is not an option. In: Proceedings of the 17th ACM workshop on hot topics in networks. HotNets'18. Association for Computing Machinery, Redmond, pp 85–91. https://doi.org/10.1145/3286062.3286075. ISBN 978-1-4503-6120-0. S2CID 53284161
9. Handley M (2019) Using ground relays for low-latency wide-area routing in megaconstellations. In: Proceedings of the 18th ACM workshop on hot topics in networks. HotNets'19. Association for Computing Machinery, Princeton, pp 125–132. https://doi.org/10.1145/3365609.3365859. ISBN 978-1-4503-7020-2. S2CID 207960066
10. Hainaut OR, Williams AP (2020) Impact of satellite constellations on astronomical observations with ESO telescopes in the visible and infrared domains. Astron Astrophys 636:A121. arXiv:2003.01992. Bibcode:2020A&A...636A.121H. https://doi.org/10.1051/0004-6361/202037501. ISSN 0004-6361. Retrieved 22 November 2020
11. Mroz P, Otarola A, Prince TA, Dekany R, Duev DA, Graham MJ, Groom SL, Masci FJ, Medford MS (2022) Impact of the SpaceX Starlink satellites on the zwicky transient facility survey observations. Astrophys J Lett. 924(2): L30. arXiv:2201.05343. Bibcode:2022ApJ...924L..30M. https://doi.org/10.3847/2041-8213/ac470a. ISSN 2041-8205
12. Lawrence A, Rawls ML, Jah M, Boley A, Di Vruno F, Garrington S, Kramer M, Lawler S, Lowenthal J, McDowell J, McCaughrean M (2022) The case for space environmentalism. Nat Astron 6(4):428–435. arXiv:2204.10025. Bibcode:2022NatAs...6..428L. https://doi.org/10.1038/s41550-022-01655-6. ISSN 2397-3366. S2CID 248300127
13. Stahl HP (2019) Multivariable parametric cost model for ground and space telescope assemblies. Bull AAS 51(7). https://baas.aas.org/pub/2020n7i143
14. Lal B, de la Rosa EB, Behrens J, Corbin B, Green EK, Picard AAJ, Balakrishnan A (2017) Global trends in small satellites. IDA Science and Technology Policy Institute, Alexandria
15. Sandaua R, Briess K, D'Errico M (2010) Small satellites for global coverage: potential and limits. ISPRS J Photogramm Remote Sens 65:492–504
16. Panga WJ, Bo B, Meng X, Yu XZ, Guo J, Zhou J (2016) Boom of the CubeSat: a statistic survey of CubeSats launch in 2003–2015. In: Proceedings of the 67th international astronautical congress (IAC), Guadalajara, Mexico, 26–30 September 2016
17. Muelhaupt TJ, Sorge ME, Morin J, Wilson RS (2019) Space traffic management in the new space era. J Space Saf Eng 85:51–60. Aerospace 2020, 7, 133 12 of 18
18. Selva D, Golkar A, Korobova O, Cruz IL, Collopy P, de Weck OL (2017) Distributed earth satellite systems: what is needed to move forward? J Aerosp Inf Syst 14:412–438
19. Lim J, Klein R, Thatcher J (2005) Good technology, bad management: a case study of the satellite phone industry. J Inf Technol Manag 16:48–55
20. Eilerten B, Krynitz M, Olafsson K (2016) New Space-Forcing a rethink of ground networks. In: Proceedings of the 14th international conference on space operations, Daejeon, Korea, 16–20 May 2016, p 2599
21. Monteverde J, Bullock M, Schulz K-J (2019) Operations Innovation. In: Proceedings of the Industry Workshop, ESA-ESOC, Darmstadt, Germany, 17–18 January 2019
22. Babrinsky N (2019) mission operations ground segments space safety. In: Proceedings of the industry workshop, ESA-ESOC, Darmstadt, Germany, 17–18 January 2019
23. Smith D, Hendrickson R (1995) Mission control for the 48-Satellite Globalstar constellation. In: Proceedings of the MILCOM'95 IEEE, San Diego, CA, USA, 5–8 November 1995, vol 2, pp 828–832
24. Howard J, Oza D, Danford SS (2006) Best practices for operations of satellite constellations. In: Proceedings of the 9th international conference on space operations, Rome, Italy, 19–24 June 2006
25. Robert RA, Ryan HT, John ML (2001) Distributed satellite constellation planning and scheduling. In: Proceedings of the FLAIRS conference AAAI, Key West, FL, USA, 21–23 May 2001, pp 68–72
26. Abramson M, Carter D, Kolitz S, Ricard M, Scheidler P (2002) Real-time optimized earth observation autonomous planning. In: Proceedings of the NASA earth science technology conference, Houston, TX, USA, 9–12 October 2002, pp 68–72
27. Jakob P, Shimizu S, Yoshikawa S, Ho K (2019) Optimal satellite constellation spare strategy using multi-echelon inventory control. J Spacecr Rocket 56:1449–1461
28. Sanchez AH, Soares T, Wolahan A (2017) Reliability aspects of mega-constellation satellites and their impact on the space debris environment. In: Proceedings of the 2017 annual reliability and maintainability symposium (RAMS), Orlando, FL, USA, 23–26 January 2017, pp 1–5
29. De Weck O, de Neufville R, Staged MC (2004) Deployment of communications satellite constellations in low earth orbit. J Aerosp Comput Inf Commun 1:119–136
30. McGrath C, Kerr E, Macdonald M (2015) An analytical, low-cost deployment strategy for satellite constellations. In: Proceedings of the 13th reinventing space conference, Oxford, UK, 10–13 November 2015
31. Crisp N, Smith K, Hollingsworth P (2015) Launch and deployment of distributed small satellite systems. Acta Astronaut 114:65–78

32. Lee HW, Jakob PC, Ho K, Shimizu S, Yoshikawa S (2018) Optimization of satellite constellation deployment strategy considering uncertain areas of interest. Acta Astronaut 153:213–228
33. Mitra RN, Agrawal DP (2015) 5G mobile technology: a survey. ICT Express 1:132–137. Aerospace 2020, 7, 133 13 of 18
34. Iera A, Molinaro A (2002) Designing the interworking of terrestrial and satellite IP-based network. IEEE Commun Mag 40:136–144
35. Chini P, Giambene G, Kota S (2009) A survey on mobile satellite systems. Int J Satell Commun Netw 28:29–57
36. Kodheli O, Gannoti A, Vanelli-Coralli A (2017) Integration of satellites in 5G through LEO constellations. In: Proceedings of the Globecomm 2017—2017 IEEE global communications conference, Singapore, 4–8 December 2017, pp 1–6
37. Pan C, Du H, Liu Q (2013) A routing algorithm for Mpls traffic engineering in Leo Satellite Constellation Network. Int J Innov Comput Inf Control 9:4139–4149
38. Hoyhtya M, Mammela A, Chen X, Hulkkonen A, Janhunen J, Dunat J-C, Gardey J (2017) Database-assisted spectrum sharing in satellite communications: a survey. IEEE Access 5:25322–25341
39. Israel D, Edwards BL, Staren JW (2017) Laser communications relay demonstration (LCRD) update and the path towards optical relay operations. In: Proceedings of the 2017 IEEE aerospace conference, Yellowstone Conference Center, Big Sky, MT, USA, 4–11 March 2017, pp 1–6
40. Muncheberg S, Gal C, Horwath J, Kinter H, Navajas LM, Soutullo M (2018) Development status and breadboard results of a laser communication terminal for large LEO constellations. In: Proceedings of the SPIE 11180, international conference on space optics—ICSO 2018, Palatanias, Greece, 9–12 October 2018
41. Nag S, Murakami D, Marker N, Lifson M, Kopardekar P (2019) Prototyping operational autonomy for space traffic management. In: Proceedings of the 70th international astronautical congress (IAC), Washington, DC, USA, 21–25 October 2019, p 16
42. Morton M, Roberts T (2011) Joint space operations center (JSpOC) mission system (JMS). In: Proceedings of the 2011 AMOS conference, Maui, HI, USA, 13–16 September 2011, p 9
43. Diserens S, Lewis HG, Fliege J (2020) IAC-19-A6.2.6: NewSpace and its implications for space debris models. J Space Saf Eng 9
44. Anz-Meador PD, Phillip D, Opiela JN, Shoots D, Liou J-C (2018) History of on-orbitsatellite fragmentations, 15th ed.; NASA Technical Reports; National Aeronautics and Space Administration, Lyndon B. Johnson Space Center, Huston, TX, USA, 4 July 2018, pp 1–637
45. Bonnal C, Ruault J-M, Desjean M-C (2013) Active debris removal: recent progress and current trends. Acta Astronaut 85:51–60
46. Felicetti L, Emami MR (2016) A multi-spacecraft formation approach to space debris surveillance. Acta Astronaut 127:491–504
47. Flohrer T, Krag H, Klinkrad H, Schildknecht T (2011) Feasibility of performing space surveillance tasks with a proposed space-based optical architecture. Adv Space Res 47:1029–1042
48. Angel F-A, Ou M, Khanh P, Steve U (2014) A review of space robotics technologies for on-orbit servicing. Prog Aerosp Sci 68:1–26
49. Infantolino GM, di Lizia P, Topputo F, Bernelli-Zazzera F (2018) On-Board Telemetry Monitoring via Support Vector Machine with Application to Philae Solar Generator. Aerotecnica Missili Spazi 97:183–188
50. Bennett JCS, Lachut M, Kooymans D, Pollard A, Smith C, Flegel S, Mockel M, O'Leary J, Samuel R, Wardman J, et al (2019) An Australian conjunction assessment service. In: Proceedings of the 2019 AMOS conference, Maui, HI, USA, 17–20 September 2019, p 9
51. Hassin JB, Iridium LK (2019) Completes historic satellite launch campaign. 11 January 2019. Aerospace 2020, 7 133 14 of 18
52. Zimmerman R, Doan D, Leung L, Mason J, Parsons N, Shaid K (2017) Commissioning the world's largest satellite constellation. In: Proceedings of the 31st annual AIAA/USU conference on small satellites, Logan, UT, USA, 5–10 August 2017
53. Weiss W, Rucinski S, Moffat A, Schwarzenberg-Czerny A, Koudelka O, Grant C, Zee R, Kuschnig R, Matthews J, Orleanski P et al (2014) BRITE-Constellation: nanosatellites for precision photometry of bright stars. Publ Astron Soc Pac 126:573–585
54. Jiang Y, Jingyin W, Zhang G, Li X, Wu J (2019) Geometric processing and accuracy verification of Zhuhai-1 hyperspectral satellites. Remote Sens 11:996
55. Glumb R, Lapsley M, Mantica P, Glumb A (2017) TRL6 testing of hyperspectral Fourier transform spectrometer instrument for CubeSat applications. In: Proceedings of the 31st annual AIAA/USU conference on small satellites, Logan, UT, USA, 5–10 August 2017
56. Polischuk GM, Kozlov V, Ilitchov V, Kozlov AG, Bartenev VA, Kossenko V, Anphimov N, Revnivykh S, Pisarev S, Tyulyakov A et al (2002) The global navigation satellite system Glonass: development and usage in the 21st century. In: Proceedings of the 34th annual precise time and time interval (PTTI) meeting, Reston, VA, USA, 3–5 December 2002, p 11
57. Zohdi TI (2019) The Game of Drones: rapid agent-based machine-learning models for multi-UAV path planning. Comput Mech. https://doi.org/10.1007/s00466-019-01761-9
58. Zohdi TI (2020) An agent-based computational framework for simulation of global pandemic and social response on planet X. Comput Mech. https://doi.org/10.1007/s00466-020-01886-2
59. Zohdi TI (2021) A digital twin framework for machine learning optimization of aerial fire fighting and pilot safety. Comput Methods Appl Mech Eng 373(1):113446
60. Zohdi TI (2022) A digital-twin and machine-learning framework for precise heat and energy management of data-centers. Comput Mech. https://doi.org/10.1007/s00466-022-02152-3
61. Zohdi TI (2022) An adaptive digital framework for energy management of complex multi-device systems. Comput Mech. https://doi.org/10.1007/s00466-022-02212-8
62. Zohdi TI (2022) A machine-learning framework for the simulation of nuclear deflection of Planet–Killer–Asteroids. Comput Methods Appl Mech Eng. https://doi.org/10.1016/j.cma.2022.115316
63. Goodrich P, Betancourt O, Arias A, Zohdi TI (2022) Placement and drone flight path mapping of agricultural soil sensors using machine learning. Comput Electron Agric. https://doi.org/10.1016/j.compag.2022.107591
64. Zohdi TI (2023) A machine-learning digital-twin for rapid large-scale solar-thermal energy system design. Comput Methods Appl Mech Eng. https://doi.org/10.1016/j.cma.2023.115991
65. Zohdi TI (2023) A voxel-based machine-learning framework for thermo-fluidic identification of unknown objects. Comput Methods Appl Mech Eng. https://doi.org/10.1016/j.cma.2023.116571
66. Holland JH (1975) Adaptation in natural & artificial systems. University of Michigan Press, Ann Arbor
67. Holland JH, Miller JH (1991) Artificial adaptive agents in economic theory (PDF). Am Econ Rev 81(2):365–371. Archived from the original (PDF) on October 27, 2005
68. Goldberg DE (1989) Genetic algorithms in search, optimization & machine learning. Addison-Wesley
69. Davis L (1991) Handbook of genetic algorithms. Thompson Computer Press
70. Onwubiko C (2000) Introduction to engineering design optimization. Prentice Hall
71. Goldberg DE, Deb K (2000) Special issue on genetic algorithms. Comput Methods Appl Mech Eng 186(2–4):121–124
72. Luenberger D (1974) Introduction to linear & nonlinear programming. Addison-Wesley, Menlo Park

73. Gill P, Murray W, Wright M (1995) Practical optimization. Academic Press
74. Hohmann W (1925) Die Erreichbarkeit der Himmelskorper. R. Oldenbourg Verlag, Munich. ISBN 3-486-23106-5
75. Bate RR, Mueller DD, White JE (1971) Fundamentals of astrodynamics (Dover books on aeronautical engineering). Dover Books
76. Lo MW, Ross SD (1997) Surfing the solar system: invariant manifolds and the dynamics of the solar system. Technical Report. IOM. JPL. pp 2–4. 312/97